# LJMU Research Online
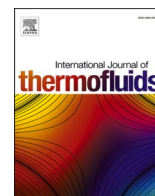
Malkeson, S, Alshaaili, S and Chakraborty, N

 Numerical investigation of steady state, laminar, natural convection of Bingham fluids in a trapezoidal enclosure heated from the bottom and cooled from the sides

http://researchonline.ljmu.ac.uk/id/eprint/24597/

Article

For more information please contact researchonline@ljmu.ac.uk

# Numerical investigation of steady state, laminar, natural convection of Bingham fluids in a trapezoidal enclosure heated from the bottom and cooled from the sides

S. Malkeson [a,*], S. Alshaaili [b], N. Chakraborty [b]

[a] School of Engineering, Liverpool John Moores University, Liverpool, L3 3AF, United Kingdom
[b] School of Engineering, Newcastle University, Newcastle-Upon-Tyne, NE1 7RU, United Kingdom

## ARTICLE INFO

## ABSTRACT

Laminar, steady-state, natural convection of Bingham fluids in trapezoidal enclosures with a heated bottom wall, cooled inclined sidewalls and an adiabatic top wall has been studied based on numerical simulations for a range of values of nominal Bingham numbers, Rayleigh numbers (i.e., $10^3 \leq Ra \leq 10^5$), and sidewall inclination angles (i.e., $30° \leq \varphi \leq 60°$) for a representative nominal Prandtl number (i.e., $Pr = 10^3$). It has been found that the mean Nusselt number $\overline{Nu}$ increases with increasing Rayleigh number $Ra$ due to the strengthening of advective transport. An increase in the sidewall inclination angle $\varphi$ leads to a decrease in the mean Nusselt number $\overline{Nu}$ due to an increase in the area for heat loss from the trapezoidal enclosure. The value of the mean Nusselt number $\overline{Nu}$ was found to decrease with increasing Bingham number $Bn$. At high values of Bingham number $Bn$, the fluid flow essentially stops within the enclosure and the heat transfer takes place primarily due to conduction and, accordingly, the mean Nusselt number $\overline{Nu}$ settles to a constant value, for a given value of sidewall inclination angle $\varphi$, irrespective of the value of nominal Rayleigh number $Ra$. Furthermore, a correlation for the mean Nusselt number $\overline{Nu}$ in trapezoidal enclosures with a heated bottom wall, an adiabatic top wall, and cooled inclined sidewalls accounting for the range of Rayleigh numbers $Ra$, Bingham numbers $Bn$ and inclined wall angles $\varphi$ considered which provides adequate approximation of the corresponding values obtained from the numerical simulations has been identified.

## 1. Introduction

Several recent studies [1–20] have focussed on the analysis of natural convection of yield stress fluids within enclosures because of their applications in food and chemical processing, nuclear waste cooling, and cryogenic storage. The yield stress fluids represent a special type of non-Newtonian fluid that acts as a solid below a threshold stress (i.e., a yield stress $\tau_y$) but flows like a fluid above this critical stress [21]. A Bingham fluid is a special type of yield stress fluid that shows a linear strain rate dependence on shear stress. The main findings of the important previous studies [1–20] on the natural convection of Bingham fluids within enclosures are summarised in Table 1. It can be seen from Table 1 that most previous analyses on the natural convection of Bingham fluids within enclosed spaces were carried out for either rectangular or axisymmetric cylindrical annular enclosures. Moreover, relatively limited attention has been directed to natural convection in

non-rectangular enclosures in comparison to the vast body of literature on natural convection in rectangular enclosures. Hussein et al. [22] analysed three-dimensional unsteady natural convection in an inclined trapezoidal air-filled enclosure and presented the variations of local and mean Nusselt numbers and demonstrated the strengthening of flow circulation with increasing Rayleigh numbers. Iyican et al. [23] analysed the natural convection of Newtonian fluids in inclined cylindrical trapezoidal enclosures which consisted of a cylindrical cold top, hot bottom walls, and plane side walls through the use of experimental and numerical means. The natural convection in trapezoidal enclosures with vertical sidewalls, an inclined cold top, and horizontal hot bottom walls was analysed by Lam et al. [24]. By contrast, the natural convection of Newtonian fluids in trapezoidal enclosures with inclined sidewalls and parallel horizontal walls was analysed by Karyakin [25]. Lee [26,27] and Peric [28] used computational means to analyse natural convection in trapezoidal enclosures with insulated horizontal top and bottom walls for Rayleigh numbers up to $10^5$ and these investigations were extended

---

* Corresponding author.
*E-mail address:* s.p.malkeson@ljmu.ac.uk (S. Malkeson).

**Nomenclature**

*Arabic*

| Symbol | Description Units |
|---|---|
| $Bn$ | Bingham number [−] |
| $C$ | Specific heat capacity [$J.kg^{-1}K^{-1}$] |
| $c_1, c_2, C_1, C_{\varphi 2}$ | Model parameter [−] |
| $e_{ij}$ | Strain rate tensor [$s^{-1}$] |
| $f_2$ | Ratio of thicknesses of hydrodynamic to thermal boundary layers [-] |
| $g$ | Acceleration due to gravity [$m.s^{-2}$] |
| $Gr$ | Grashof number [−] |
| $h$ | Heat transfer coefficient [$W.m^{-2}.K^{-1}$] |
| $H$ | Height of the trapezoidal enclosure [$m$] |
| $k$ | Thermal conductivity [$W.m^{-1}.K^{-1}$] |
| $L$ | Length of heated bottom wall of trapezoidal enclosure [$m$] |
| $min$ | Minimum value [−] |
| $max$ | Maximum value [−] |
| $Nu$ | Local Nusselt number [−] |
| $\overline{Nu}$ | Mean Nusselt number [−] |
| $p$ | Pressure [$kg.m^{-1}.s^{-2}$] |
| $Pr$ | Prandtl number [−] |
| $q_w$ | Heat flux at the bottom wall [$W.m^{-2}$] |
| $R^2$ | Coefficient of determination [−] |
| $Ra$ | Rayleigh number [−] |

| Symbol | Description Units |
|---|---|
| $T$ | Temperature [$K$] |
| $T_c$ | Temperature of the cooled inclined sidewalls [$K$] |
| $T_H$ | Temperature of the heated bottom wall [$K$] |
| $u_i{}^{th}$ | component of velocity $u$ [$m.s^{-1}$] |
| $U_2$ | Dimensionless vertical velocity ($u_2.L/\alpha$) [−] |
| $x_i{}^{th}$ | component of spatial coordinate $x$ [$m$] |

*Greek*

| Symbol | Description Units |
|---|---|
| $\alpha$ | Thermal diffusivity [$m^2.s^{-1}$] |
| $\beta$ | Thermal expansion coefficient [$K^{-1}$] |
| $\delta$ | Hydrodynamic boundary layer thickness [m] |
| $\delta_{th}$ | Thermal boundary layer thickness [m] |
| $\delta_{ij}$ | Kronecker delta [-] |
| $\rho$ | Density [$kg.m^{-3}$] |
| $\mu$ | Dynamic viscosity [$kg.m^{-1}s^{-1}$] |
| $\vartheta$ | Characteristic vertical velocity component [$ms^{-1}$] |
| $\tau$ | Shear stress [$kg.m^{-1}.s^{-2}$] |
| $\tau_y [kg.m^{-1}.s^{-2}]$ | Yield shear stress |
| $\varphi$ | Inclination angle of trapezoidal enclosure sidewall [°] |
| $\psi$ | Stream function [$m^2.s^{-1}$] |
| $\Psi$ | Non-dimensional stream function [−] |
| $\theta$ | Non-dimensional temperature [−] |
| $\tau_{ij}$ | Stress tensor [$kg.m^{-1}.s^{-2}$] |
| $\Delta T$ | Temperature difference between the hot and cold walls [$K$] |

by Sadat and Salagnac [29] and Kuyper and Hoogendoorn [30] for larger Rayleigh number values. The natural convection within trapezoidal enclosures with several different configurations consisting of baffles and partitions has been analysed by Moukalled and Acharya [31–33] and Moukalled and Darwish [34]. Furthermore, da Silva et al. [35] analysed the effects of Prandtl number, and Rayleigh number, as well as the inclination angle of the top wall on the natural convection of Newtonian fluids within trapezoidal enclosures with baffles and partitions, and they utilised the simulation data to propose a correlation for the mean Nusselt number. The natural convection of Newtonian fluids in trapezoidal enclosures with a bottom wall subjected to a uniform heat flux and linearly heated sidewalls with an insulated top wall was numerically analysed by Basak et al. [36] and the effects of wall inclination on the heat transfer rate were discussed in detail. Tracy and Crunkleton [37] used numerical simulations to analyse the unsteady natural convection of Newtonian fluids in an isosceles trapezoidal enclosure with differentially heated horizontal walls heated from below and discussed the flow characteristics and its impact on the heat transfer process. Mehryan et al. [38] analysed the natural convection of Newtonian fluids within a trapezoidal enclosure with a flexible partition for different Rayleigh numbers and also analysed the flow-induced stresses on the flexible partition.

Several studies focussed on the heat transfer behaviour for natural convection in Newtonian nanofluids in trapezoidal enclosures. Haq et al. [39] analysed the natural convection of water-based carbon nanotubes in trapezoidal enclosures that are partially heated from the horizontal bottom wall and are cooled by inclined sidewalls, reporting an increase in heat transfer due to carbon nanotubes [39]. They subsequently extended this work to account for water-based CuO nanofluids within a trapezoidal enclosure where a heated obstacle is positioned at the centre of the enclosure [40] and found that the rate of heat transfer decreases with increasing volume fraction of CuO nanoparticles. Saleh et al. [41] reported heat transfer augmentations due to the presence of nanoparticles for the natural convection of water–$Al_2O_3$ and water–Cu nanofluids in trapezoidal enclosures with differentially heated inclined sidewalls. The Rayleigh-Bénard convection (i.e., a heated bottom wall and a cooled top wall with adiabatic inclined side walls) of carbon

nanotubes in trapezoidal enclosures was analysed by Esfe et al. [42] and indicated that the mean Nusselt number decreases with an increasing inclination angle of the sidewalls for small Rayleigh number values ($\leq 10^4$), however, a non-monotonic trend of the mean Nusselt number with inclination angle for large Rayleigh numbers ($\sim 10^6$) was observed for all solid volume fractions.

To date, relatively limited effort has been directed to the study of the natural convection of non-Newtonian fluids in trapezoidal enclosures. Aghighi et al. [20] recently analysed Rayleigh–Bénard convection within trapezoidal enclosures filled with viscoplastic fluid for a range of values of the angle of inclination of the side walls $\varphi$, nominal Rayleigh number $Ra$ and nominal Prandtl number $Pr$. Recently, Malkeson et al. [43] analysed the natural convection of non-Newtonian power-law fluids within a trapezoidal enclosure with a heated bottom wall, cooled inclined sidewalls and an adiabatic top wall for different values of power-law indices, nominal Rayleigh and Prandtl numbers based on computational simulations and proposed a correlation for the mean Nusselt number. However, the natural convection in Bingham fluids in a trapezoidal enclosure with a heated bottom wall, an adiabatic top wall, and cooled inclined sidewalls, to the best of the authors' knowledge, is yet to be considered in detail. Accordingly, the aims and objectives of the present study are, as follows:

1. To investigate the effect of the Rayleigh number $Ra$, the Bingham number $Bn$, and the geometry of a trapezoidal cavity on the natural convection behaviour in Bingham fluids in a trapezoidal enclosure with a heated bottom wall, an adiabatic top wall and cooled inclined sidewalls.

2. To identify an expression for the mean Nusselt number $\overline{Nu}$ for the current configuration across the considered range of Rayleigh number $Ra$, Bingham number $Bn$ and sidewall inclination angle $\varphi$.

The rest of the paper will be organised in the following manner. The mathematical background and numerical implementation pertaining to the current analysis are presented in the next section. Following that, results are presented and subsequently discussed. The main findings are summarised, and conclusions are drawn in the final section of this paper.

## 2. Mathematical background and numerical implementation

A schematic of the configuration used in the current analysis is given in Fig. 1a where $H$ is the height of the trapezium, $L$ is the length of the bottom heated wall, and $\varphi$ is the inclination angle of the sidewall. The heated bottom wall is maintained at a temperature $T_H$. The two inclined sidewalls are maintained at a temperature $T_C$. In the current analysis, it is assumed that $T_H > T_C$. The top wall is taken to be adiabatic in nature. For all walls, the no-slip condition is applied. The flow is assumed to be laminar, steady, incompressible, and two-dimensional in nature (i.e., the physical flow domain is considered to be an infinitely long channel and, subsequently, the third dimension is assumed to not affect the flow field). For the current study, the conservation equations for mass, momentum, and energy take the following form:

$$\frac{\partial u_i}{\partial x_i} = 0 \tag{1i}$$

$$\rho u_j \left(\frac{\partial u_i}{\partial x_j}\right) = -\left(\frac{\partial p}{\partial x_i}\right) + \delta_{2i}\rho g \beta (T_H - T_C) + \frac{\partial \tau_{ij}}{\partial x_j} \tag{1ii}$$

$$\rho u_j C \left(\frac{\partial T}{\partial x_j}\right) = k \left(\frac{\partial^2 T}{\partial x_j \partial x_j}\right) \tag{1iii}$$

where $p$ is the pressure, $\rho$ is the density, $u_i$ ($x_i$) is the $i^{th}$ component of velocity (spatial coordinate), $g$ is acceleration due to gravity, $\beta$ is the thermal expansion coefficient, $\tau_{ij}$ is the stress tensor, $T$ is the temperature, $C$ is the specific heat, and $k$ is the thermal conductivity. In Eq. 1ii, the Kronecker delta $\delta_{2i}$ is used to ensure that the buoyancy effect occurs in the vertical direction (i.e., $x_2$ direction) only. The Bingham model for a yield stress fluid can be expressed as [21]:

$$\underline{\dot{\gamma}} = 0 \text{ for } \tau \leq \tau_y \tag{2i}$$

$$\underline{\tau} = \left(\mu + \tau_y / \dot{\gamma}\right)\dot{\gamma}_{ij} \text{ for } \tau > \tau_y \tag{2ii}$$

where the components of the strain rate tensor $\dot{\gamma}$ are given by: $\dot{\gamma}_{ij} = (\partial u_i / \partial x_j + \partial u_j / \partial x_i)$. In Eq. 2, $\tau = \left[0.5(\underline{\tau} : \underline{\tau})\right]^{0.5}$ and $\dot{\gamma} = \left[0.5(\underline{\dot{\gamma}} : \underline{\dot{\gamma}})\right]^{0.5}$ are the magnitudes of shear stress and strain rate, respectively. The stress-shear rate characteristics of a Bingham fluid are approximated

**Table 1**
Summary of the findings of existing analyses on natural convection of yield stress fluids in enclosed spaces. CWT and CWHF stand for constant wall temperature and constant wall heat flux boundary conditions.

| Ref. | Type | Enclosure | Configuration & Boundary conditions | $AR = H/L$ | Model & Fluid | Ra, Pr | | Correlation |
|------|------|-----------|-------------------------------------|------------|---------------|--------|--|-------------|
| Zhang et al. [1] | A, N | Square | Diff. heated horizontal wall (CWT) | 1 | Bingham | $Ra_{crit}$ for $\overline{Nu} > 1$ | $Pr = 1$ | - |
| Balmforth and Rust [2] | A,N, E | - | Diff. heated horizontal layers (CWT) | - | Bingham Bi-viscosity reg. Carbopol gel | $Ra_{crit}$ for $\overline{Nu} > 1$ | | - |
| Vikhansky [3] | N | Square | Diff. heated horizontal wall (CWT) | 1 | Bingham | $Ra_{crit}$ for $\overline{Nu} > 1$ | | - |
| Vikhansky [4] | N | Rectangular | Diff. heated horizontal wall (CWT) | $0.5 \leq AR \leq 5$ | Bingham | $Ra_{crit}, Bn_{crit}$ for $\overline{Nu} > 1$ | | $Bn_{crit} = f(Bn, AR)$ |
| Turan et al. [5] | N | Rectangular | Diff. heated horizontal wall comparison (CWT-CWHF) | $0.25 \leq AR \leq 4$ | Bi-viscosity reg. | $Ra_{crit}$ for $\overline{Nu} > 1$ | | $Ra_{crit} = f(Bn, Pr, AR)$ |
| Darbouli et al. [6] | E | Rectangular | Diff. heated horizontal wall (CWT) | $6 \leq AR \leq 17.9$ | Carbopol gel | $Bn_{crit}$ for $\overline{Nu} > 1$ | | - |
| Kebiche et al. [7] | E | Rectangular | Diff. heated horizontal wall (CWT) | 19.3 | Carbopol gel | $Bn_{crit}$ for $\overline{Nu} > 1$ | | - |
| Turan et al. [8] | N | Square | Diff. heated horizontal wall (CWT) | 1 | Bi-viscosity reg. | $10^3 \leq Ra \leq 10^5$ | $0.1 \leq Pr \leq 10^2$ | $\overline{Nu} = f(Ra, Pr, Bn)$ |
| Turan et al. [9] | N | Square | Diff. heated horizontal wall comparison (CWT-CWHF) | 1 | Bi-viscosity reg. | $10^3 \leq Ra \leq 10^5$ | $0.1 \leq Pr \leq 10^2$ | $\overline{Nu} = f(Ra, Pr, Bn)$ |
| Yigit et al. [10] | N | Square $0^o \leq \phi \leq 180^o$ | Diff. heated inclined horizontal wall (CWT) | 1 | Bi-viscosity reg. | $10^3 \leq Ra \leq 10^5$ | $Pr = 500$ | $\overline{Nu} = f(Ra, Pr, Bn, \phi)$ |
| Yigit et al. [11] | N | Rectangular | Diff. heated horizontal wall (CWT) | $0.25 \leq AR \leq 4$ | Bi-viscosity reg. | $10^3 \leq Ra \leq 10^5$ | $Pr = 500$ | $\overline{Nu} = f(Ra, Pr, Bn, AR)$ |
| Yigit and Chakraborty [12] | N | Rectangular | Diff. heated horizontal wall comparison (CWT-CWHF) | $0.25 \leq AR \leq 4$ | Bi-viscosity reg. | $10^3 \leq Ra \leq 10^5$ | $Pr = 500$ | $\overline{Nu} = f(Ra, Pr, Bn, AR)$ |
| Hassan et al. [13] | E,N | Square | Diff. heated horizontal wall (CWHF) | 1 | Carbopol gel Herschel-Bulkley | $10^4 \leq Ra \leq 10^6$ | | $\overline{Nu} = f(Ra, Y_o)$ |
| Yigit et al. [14] | N | Cylindrical annular $0 \leq r_i/L \leq 24$ | Diff. heated horizontal wall comparison (CWT-CWHF) | 1 | Bi-viscosity reg. | $Pr = 500$ | | $\overline{Nu} = f(Ra, Pr, Bn, r_i/L)$ |
| Yigit and Chakraborty [15] | N | Cylindrical annular $0.125 \leq r_i/L \leq 16$ | Diff. heated vertical wall (CWHF) | 1 | Bi-viscosity reg. | $10^3 \leq Ra \leq 10^6$ | $10 \leq Pr \leq 10^3$ | $\overline{Nu} = f(Ra, Pr, Bn, r_i/L)$ |
| Yigit et al. [16] | N | Cylindrical annular $0.125 \leq r_i/L \leq 16$ | Diff. heated vertical wall comparison (CWT-CWHF) | 1 | Bi-viscosity reg. | $10^3 \leq Ra \leq 10^6$ | $10 \leq Pr \leq 10^3$ | $\overline{Nu} = f(Ra, Pr, Bn, r_i/L)$ |
| Yigit and Chakraborty [17] | N | Cylindrical annular | Diff. heated horizontal wall comparison (CWT-CWHF) | $1/4 \leq AR \leq 4$ | Bi-viscosity reg. | $Pr = 500$ | | $\overline{Nu} = f(Ra, Pr, Bn, r_i/L)$ |
| Yigit and Chakraborty [18] | N | Cylindrical annular | Diff. heated vertical wall comparison (CWT-CWHF) | $1/8 \leq AR \leq 8$ | Bi-viscosity reg. | $Pr = 500$ | | $\overline{Nu} = f(Ra, Pr, Bn, r_i/L, AR)$ |
| Yigit et al. [19] | N | Rectangular | Rayleigh-Benard convection (CWT) | 1 | Bi-viscosity reg. | $Pr = 320$ | $Ra = 10^7, 10^8$ | - |
| Aghighi et al. [20] | N | Trapezoidal | Rayleigh-Benard convection (CWT) | 1 | Papanastasiou reg. | $Pr = 500$ | $5 \times 10^3 \leq Ra \leq 10^5$ | $\overline{Nu} = f(Ra, Pr, Bn)$ |

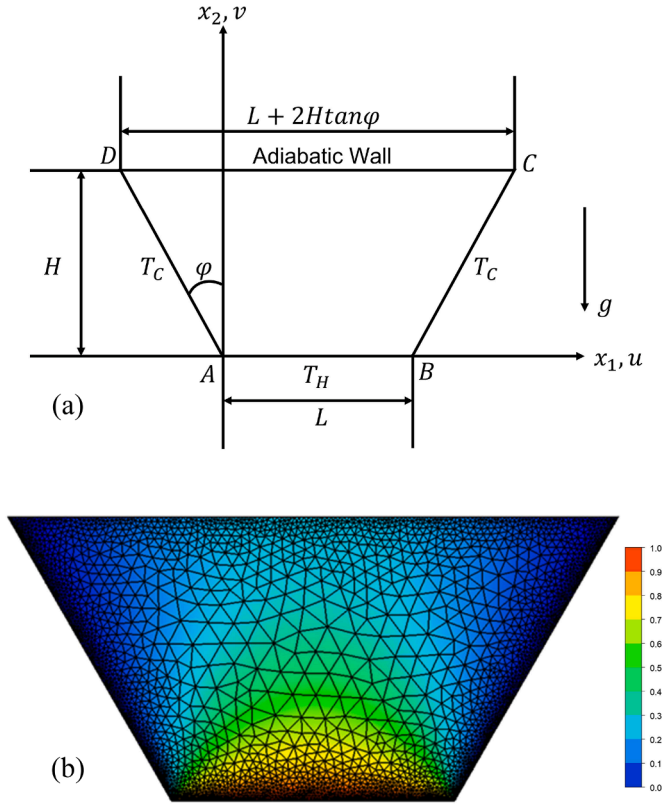A: analytical; E: experimental; N: numerical

**Fig. 1.** (a) Schematic of considered configuration, and (b) the non-dimensional temperature $\theta = (T - T_C)/(T_H - T_C)$ field for the $Ra = 10^3$, $Bn = 0.5$, $\varphi = 30°$ case with the mesh superimposed.

here by the bi-viscosity regularisation [44]:

$$\underline{\underline{\tau}} = \mu_{yield}\underline{\dot{\gamma}} \text{ for } \dot{\gamma} \leq \tau_y/\mu_{yield} \tag{3i}$$

$$\underline{\underline{\tau}} = \tau_y\left(\underline{\dot{\gamma}}/\dot{\gamma}\right) + \mu\underline{\dot{\gamma}} \text{ for } \dot{\gamma} > \tau_y/\mu_{yield} \tag{3ii}$$

where $\mu_{yield}$ is the yield viscosity and $\mu$ is the plastic viscosity such that the solid material is represented by a high-viscosity fluid [42]. According to its proponents [42], a value of $\mu_{yield} \geq 1000\mu$ satisfactorily mimics the true Bingham model, and here $\mu_{yield}/\mu = 10^4$ is chosen to ensure the high fidelity of the computational results. It has been demonstrated elsewhere [15] that the results obtained for natural convection of Bingham fluids are not too sensitive to the choice of regularisation and a regularisation proposed by Papanastasiou [45] (i.e., $\underline{\underline{\tau}} = \tau_y(1 - \exp(-m\dot{\gamma})) + \mu\underline{\dot{\gamma}}$ with large values of $m$ such as $m = 10^4 L\rho C/k$ [15]) has been found to provide similar results with a difference (~1–2 %), which is much smaller than typical experimental uncertainty. All regularisations effectively transform the "unyielded" region to a zone of high viscosity and therefore no extra benefit can be expected as a result of the usage of an alternative regularisation. The plastic viscosity $\mu$ and yield stress $\tau_y$ are taken to be independent of temperature for the sake of simplicity. These assumptions are consistent with experimental evidence [46] that the yield stress is approximately independent of temperature and the plastic viscosity shows only a weak temperature dependence (similar to Newtonian fluids) for Carbopol (i.e., a yield stress fluid which is often used for laboratory scale experiments) in the temperature range 0° to 90 °C.

The Nusselt number $Nu$ (defined as $Nu = hL/k$ where $h = q_w/(T_H - T_C)$ is the local heat transfer coefficient where $q_w$ is the wall heat

flux at the bottom hot wall) can be expressed in this configuration, according to Buckingham's pi theorem, as $Nu = f(Ra, Pr, H/L, \varphi, Bn)$ where the Rayleigh number $Ra$, Prandtl number $Pr$, and Bingham number $Bn$, are defined as $Ra = \rho g\beta\Delta TL^3/(\mu\alpha)$, $Pr = C\mu/k$, and $Bn = \tau_y L/(\mu\sqrt{g\beta\Delta TL})$ where $\Delta T = (T_H - T_C)$, and $\alpha = k/\rho C$ is the thermal diffusivity. For the present analysis, the aspect ratio $H/L$ is considered to be unity (i.e., $H/L = 1.0$). A detailed scaling analysis to predict the vertical velocity component, hydrodynamic and thermal boundary layer thicknesses, and Nusselt number in the case of natural convection of Bingham fluids within enclosed spaces was presented elsewhere along with their derivations [5,8] and, thus, is not repeated here but the summary of that scaling analysis is presented in Table 2.

For the current study, a finite-volume (i.e., Ansys-FLUENT) solver [47] has been employed for solving the governing equations. A second-order upwind scheme (second-order central difference) has been used for the discretisation of convective (diffusive) terms. The coupling of velocity and pressure components is achieved using the SIMPLE (Semi-Implicit Method for Pressure-Linked Equations) algorithm [48]. The convergence criteria, for all cases, were set to $10^{-6}$ for all relative (scaled) residuals. The boundary conditions, for the current analysis, are: $u_1 = u_2 = 0$, $T = T_H$ at the bottom wall; $u_1 = u_2 = 0$, $\partial T/\partial y = 0$ at the top wall; and $u_1 = u_2 = 0$, $T = T_C$ at the sidewalls. In the current study, the parameters considered are: $Ra = 10^3, 10^4, 10^5$; and $\varphi = 30°$, $45°$, $60°$ for a single representative value of Prandtl number $Pr = 10^3$ (e.g., 0.2 % by mass Carbopol solution in water shows a Prandtl number of about 1000 when the flow is approximated by the Bingham plastic model) and this choice of $Pr$ is consistent with previous analyses [15,16]. The Bingham number $Bn$ has been varied from $Bn = 0$ (i.e., Newtonian fluid) to $Bn = Bn_{max}$ for a given set of values of $Ra$, $\varphi$ and $Pr$ such that the mean Nusselt number $\overline{Nu}$ becomes insensitive to any change in Bingham number for $Bn \geq Bn_{max}$. A mesh independence analysis has been completed and a non-uniform unstructured triangular mesh of 22,500 cells is used for the study, as shown in Fig. 1b. In the mesh sensitivity study, four mesh sizes were considered: 1. M1 (i.e., $50 \times 50$ cells), 2. M2 (i.e., $100 \times 100$ cells), 3. M3 (i.e., $150 \times 150$ cells), and 4. M4 (i.e., $200 \times 200$ cells). Moreover, four different types of mesh structures were considered: 1. non-uniform unstructured triangular mesh, 2. structured triangular mesh, 3. unstructured quadrilateral mesh, and 4. structured quadrilateral mesh. Furthermore, the bias factor towards the heated bottom wall and cooled inclined sidewalls was varied with the lowest relative error between M3 and M4 for the mean Nusselt number $\overline{Nu}$ on the heated bottom wall being observed for a bias factor of 1.25 in the unstructured triangular mesh. The considered mesh of 22,500 cells provides agreement of $\overline{Nu}$ on the heated bottom wall to within 2 % with a mesh of 30,625 cells but with a reduction in computational cost of 26%, offering a balance between cost and accuracy for the parametric investigation where more than 125 simulations were considered.

**Table 2**
The scaling estimates of wall heat flux $q$, Nusselt number $Nu$, characteristic vertical velocity $\vartheta$, and hydro-dynamic and thermal boundary layer thicknesses (i.e., $\delta$ and $\delta_{th}$) according to the analysis by Turan et al. [8,9]. The function $f_2(Ra, Pr, Bn, \varphi)$ represents the ratio of $\delta/\delta_{th}$.

| Quantities | Scaling relations |
|---|---|
| Wall heat flux ($q$) | $q \sim k\Delta T/\delta_{th} \sim h\Delta T$ |
| Nusselt number ($Nu$) | $Nu \sim hL/k \sim L/\delta_{th}$ or $Nu \sim (L/\delta)f_2(Ra, Pr, Bn, \varphi)$ |
| Characteristic vertical velocity ($\vartheta$) | $\vartheta \sim \sqrt{g\beta\Delta TL} \sim (\mu/\rho L)\sqrt{Ra/Pr}$ |
| Hydrodynamic boundary layer ($\delta$) | $\delta \sim \dfrac{\mu/\rho}{\sqrt{g\beta\,\Delta T\,L}}\left[\dfrac{Bn}{2} + \dfrac{1}{2}\sqrt{Bn^2 + 4\left(\dfrac{Ra}{Pr}\right)^{1/2}}\right]$ |
| Thermal boundary layer ($\delta_{th}$) | $\delta_{th} \sim \min\left[L, \dfrac{LPr^{1/2}}{f_2(Ra, Bn, Pr, \varphi)Ra^{1/2}}\left[\dfrac{Bn}{2} + \dfrac{1}{2}\sqrt{Bn^2 + 4\left(\dfrac{Ra}{Pr}\right)^{1/2}}\right]\right]$ |

The non-dimensional temperature $\theta = (T - T_C)/(T_H - T_C)$ field of an example case (i.e., $Ra = 10^3$, $Bn = 0.5$, $\varphi = 30°$) is also provided in Fig. 1b. Furthermore, the currently considered numerical implementations have been tested against benchmarks involving the natural convection of Newtonian fluids in a square enclosure (i.e., $\varphi = 0°$) with differentially heated sides [49] and the natural convection in partially divided trapezoidal cavities [34]. For both benchmark studies, satisfactory agreements were obtained (i.e., typically within 0.5% but, at most, 2% across all of the benchmark cases considered). Further information on the benchmarking for natural convection of Newtonian fluids within trapezoidal enclosures can be found in a previous publication by the present authors [43].

The present numerical set up was previously used by Turan et al. [5, 8] for natural convection of Bingham fluids and interested readers are referred to [5–12,14–19] for further information in this regard. The mean Nusselt number obtained from the current numerical simulation methodology has been found to be within 3% of the values reported by Vola et al. [50] for natural convection of Bingham fluids within square enclosures with differentially heated vertical walls for $Ra = 10^4$, $10^5$ and $10^6$ with $Pr = 1.0$. Furthermore, the present numerical set up has been benchmarked in comparison to Aghighi et al. [20] who investigated Rayleigh–Bénard convection of a viscoplastic liquid in a trapezoidal enclosure for varying Rayleigh number $Ra$ (i.e., $Ra = 5 \times 10^3$, $10^4$, $5 \times 10^4$, $10^5$), sidewall inclination angle $\varphi$ (i.e., $\varphi = 15°$, $30°$, $45°$, $60°$) for $Pr = 500$ across a range of Yield numbers $Y$ (i.e., $Y = \tau_y/(\rho\beta g\Delta TH)$ where $H$ is the height of the trapezoidal cavity). Excellent agreement (i.e., with 2%) has been observed with the values of the mean Nusselt number $\overline{Nu}$ on the hot wall from Aghighi et al. [20] across a range of Rayleigh numbers $Ra$ and sidewall inclination angles $\varphi$ for the currently considered numerical set up. A summary of the findings of the benchmarking with Aghighi et al. [20] is provided in Table 3.

## 3. Results & discussion

In the following sections, the effects of Rayleigh number $Ra$, Bingham number $Bn$, and inclination angle $\varphi$ on the heat transfer behaviour in the trapezoidal enclosure are discussed.

### 3.1. Variations in local Nusselt number

Fig. 2a–c show the variations of the local Nusselt number $Nu$ on the hot wall with normalised horizontal distance $x_1/L$ for Rayleigh number $Ra = 10^3$, $10^4$ and $10^5$ and $Pr = 10^3$ are shown for $\varphi = 30°$, $45°$, and $60°$, respectively. The results for $Bn = 0.5$ are compared to the corresponding Newtonian fluid (i.e., $Bn = 0$ where the yield stress $\tau_y = 0$) results in Fig. 2a–c. Fig. 2a–c show that the Nusselt number $Nu$ increases with increasing Rayleigh number $Ra$ for both the Newtonian and Bingham fluids considered. Moreover, Fig. 2a–c show that the values of the Nusselt number $Nu$ are generally greater for the Newtonian fluid cases than those in the Bingham fluid cases for the same nominal Rayleigh number $Ra$. This difference is most apparent in Rayleigh number $Ra = 10^5$ cases and is because of the strengthening of buoyancy effects with increasing $Ra$ which will have the greatest effect in the Newtonian (i.e., $Bn = 0$) cases where the yield stress is $\tau_y = 0$.

The local Nusselt number assumes high values at the ends of the horizontal heated wall and the value of $Nu$ gradually decreases towards the middle of the horizontal wall. The middle of the bottom wall is the farthest away from the cold inclined walls. Thus, the wall normal temperature gradients are smaller at that location in comparison to the ends of the bottom wall which experience a stronger thermal gradient due to the proximity of the cooled inclined walls. This is reflected in the gradual drop of $Nu$ from both ends of the hot bottom wall towards the centre, which can further be explained based on distributions of streamlines and non-dimensional temperature $\theta$ contours within the enclosure.

**Table 3**
Comparison of the variation of $\overline{Nu}$ with Yield number $Y$ on the heated bottom wall of Rayleigh-Bernard convection for the currently considered numerical set up and the results of Aghighi et al. [20] for different Rayleigh numbers $Ra$ and sidewall inclination angles $\varphi$.

| $Ra$ | $\phi$ (°) | $Y$ | Aghighi et al. [20] | Present study | % Diff. |
|---|---|---|---|---|---|
| 5000 | 30 | 0 | 2.43 | 2.43 | -0.29 |
| 5000 | 30 | 0.0005 | 2.38 | 2.39 | -0.34 |
| 5000 | 30 | 0.001 | 2.33 | 2.34 | -0.66 |
| 5000 | 30 | 0.0015 | 2.28 | 2.29 | -0.43 |
| 5000 | 30 | 0.002 | 2.23 | 2.24 | -0.13 |
| 5000 | 30 | 0.0025 | 2.17 | 2.18 | -0.40 |
| 5000 | 30 | 0.003 | 2.11 | 2.11 | -0.02 |
| 5000 | 30 | 0.0035 | 2.04 | 2.04 | 0.07 |
| 5000 | 30 | 0.004 | 1.97 | 1.96 | 0.62 |
| 5000 | 30 | 0.0045 | 1.85 | 1.85 | 0.15 |
| 5000 | 30 | 0.00474 | 1.80 | 1.77 | 1.81 |
| 5000 | 30 | 0.00505 | 1.40 | 1.41 | -0.73 |
| 5000 | 60 | 0 | 3.23 | 3.29 | -1.85 |
| 5000 | 60 | 0.0009 | 3.16 | 3.23 | -2.02 |
| 5000 | 60 | 0.0018 | 3.10 | 3.15 | -1.88 |
| 5000 | 60 | 0.0027 | 3.03 | 3.08 | -1.74 |
| 5000 | 60 | 0.0036 | 2.95 | 3.00 | -1.68 |
| 5000 | 60 | 0.0045 | 2.86 | 2.92 | -1.90 |
| 5000 | 60 | 0.0054 | 2.78 | 2.82 | -1.50 |
| 5000 | 60 | 0.0063 | 2.68 | 2.72 | -1.45 |
| 5000 | 60 | 0.0072 | 2.57 | 2.60 | -1.26 |
| 5000 | 60 | 0.00787 | 2.48 | 2.46 | 0.90 |
| 5000 | 60 | 0.00883 | 1.63 | 1.62 | 0.62 |
| 100000 | 30 | 0 | 6.20 | 6.19 | 0.03 |
| 100000 | 30 | 0.0015 | 5.93 | 5.93 | 0.08 |
| 100000 | 30 | 0.003 | 5.68 | 5.66 | 0.23 |
| 100000 | 30 | 0.0045 | 5.41 | 5.42 | -0.10 |
| 100000 | 30 | 0.006 | 5.18 | 5.17 | 0.18 |
| 100000 | 30 | 0.0075 | 4.94 | 4.93 | 0.12 |
| 100000 | 30 | 0.009 | 4.69 | 4.68 | 0.13 |
| 100000 | 30 | 0.0105 | 4.45 | 4.42 | 0.67 |
| 100000 | 30 | 0.012 | 4.18 | 4.14 | 1.00 |
| 100000 | 30 | 0.0135 | 3.87 | 3.80 | 1.84 |
| 100000 | 30 | 0.015 | 3.37 | 3.36 | 0.45 |
| 100000 | 30 | 0.01572 | 3.09 | 3.00 | 2.97 |
| 100000 | 30 | 0.01615 | 1.39 | 1.40 | -0.43 |
| 100000 | 60 | 0 | 7.51 | 7.61 | -1.26 |
| 100000 | 60 | 0.0022 | 7.12 | 7.19 | -0.97 |
| 100000 | 60 | 0.0044 | 6.65 | 6.74 | -1.37 |
| 100000 | 60 | 0.0066 | 6.18 | 6.29 | -1.77 |
| 100000 | 60 | 0.0088 | 5.73 | 5.84 | -1.82 |
| 100000 | 60 | 0.011 | 5.26 | 5.39 | -2.48 |
| 100000 | 60 | 0.0132 | 4.84 | 4.96 | -2.42 |
| 100000 | 60 | 0.0154 | 4.44 | 4.54 | -2.19 |
| 100000 | 60 | 0.0176 | 3.96 | 4.08 | -2.88 |
| 100000 | 60 | 0.01897 | 3.54 | 3.57 | -0.76 |
| 100000 | 60 | 0.02108 | 1.65 | 1.68 | -1.55 |

### 3.2. Streamline behaviour

Fig. 3a-–i and 4a-i show the streamline distributions across the Rayleigh numbers considered (i.e., $Ra = 10^3$, $10^4$, and $10^5$) at $Bn = 0.0$, 0.1 and 0.5 and $Pr = 10^3$ for $\varphi = 30°$ and $\varphi = 60°$, respectively. Given the symmetrical nature of the boundary conditions employed in the current configuration, the streamlines are found to be symmetrical about the central $x_1$ location for the cases considered. In all cases, the streamlines indicate counter-rotating cells within the enclosure where there is one cell in the left half and there is one cell in the right half. The flows in the left and right halves have been observed to be identical in magnitude but in opposite directions of rotation with the fluid ascending along the vertical line of symmetry of the enclosure, subsequently impinging with the adiabatic top wall before moving to the sides and interacting with the cooled sidewalls and descending. These observations are consistent with previous analyses of laminar natural convection in trapezoidal enclosures with heating from the bottom and symmetrical cooling from the sidewalls [43].
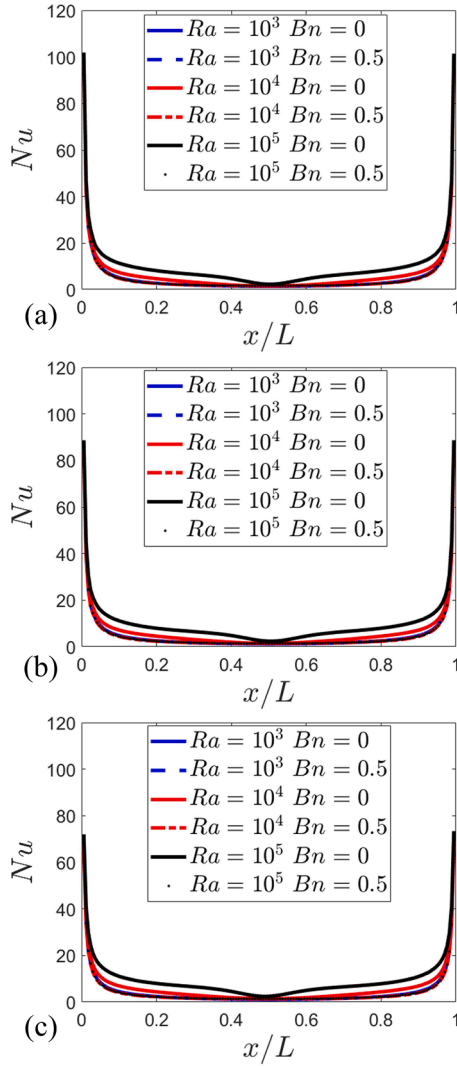
**Fig. 2.** The variations of local Nusselt number $Nu$ on the hot bottom wall with normalised horizontal distance $x_1/L$ for (a) $Ra = 10^3$, $Ra = 10^4$ and $Ra = 10^5$ where $Bn = 0.5$, $Pr = 10^3$ compared to the corresponding Newtonian fluid for (a) $\varphi = 30°$, (b) $\varphi = 45°$ and (c) $\varphi = 60°$ configurations.

### 3.3. Behaviour of non-dimensional temperature θ

Fig. 5a–i and 6a–i show the contours of non-dimensional temperature θ across the Rayleigh numbers considered (i.e., $Ra = 10^3$, $10^4$, and $10^5$) at $Bn = 0.0$, 0.1 and 0.5 and $Pr = 10^3$ for $\varphi = 30°$ and $\varphi = 60°$, respectively. It can be appreciated from Figs. 5 and 6 that the thickness of the thermal boundary layer $\delta_{th}$ on top of hot and cold walls decreases with increasing Rayleigh number $Ra$, which is reflected in the increase in $Nu \sim L/\delta_{th}$ [5,8] with an increase in $Ra$. Moreover, it can be seen from Figs. 5 and 6 that the thermal boundary layer thickness on the bottom hot wall increases towards its middle, which is consistent with the drop of $Nu \sim L/\delta_{th}$ [5,8] from the edge towards the centre of the horizontal bottom wall. Figs. 5 and 6 also show that the thermal boundary layer for the Bingham fluid case is thicker than the Newtonian fluid case, which is reflected in the reduction of $Nu \sim L/\delta_{th}$ [5,8] with an increase in Bingham number $Bn$ for a given set of values of $Ra$ and $Pr$, as observed in Fig. 2. Figs. 5 and 6 further show that the contours of non-dimensional temperature θ become increasingly curved with an increase in Rayleigh number $Ra$, which is indicative of the strengthening of advective transport. Moreover, the isotherms are less curved in the Bingham fluid cases in comparison to the Newtonian fluid case for a given set of values of $Ra$ and $Pr$, which is indicative of the weakening of advective transport

and strengthening of thermal diffusion with an increase in Bingham number $Bn$. This suggests that for sufficiently large values of Bingham number $Bn$ conduction begins to play the dominant role in thermal transport and, at that stage, any change in Rayleigh number $Ra$ no longer influences the value of the Nusselt number $Nu$.
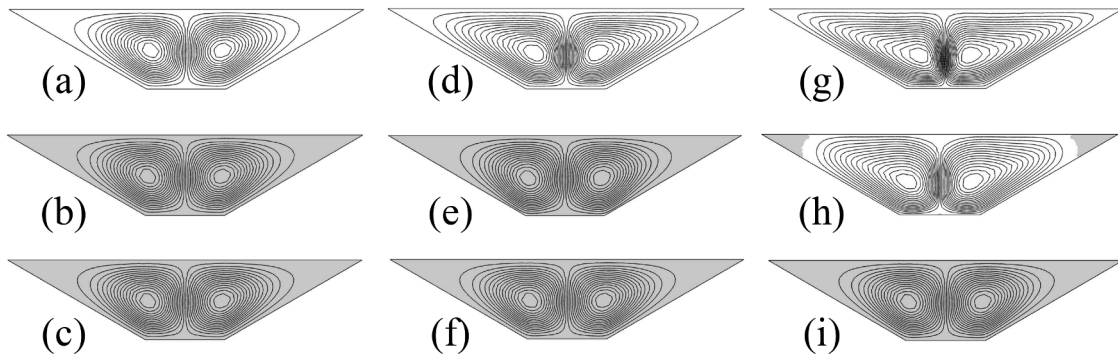
### 3.4. Apparently unyielded regions (AUR)

Fig. 3a–i and 4a–i also show the "unyielded" zones (i.e., the regions defined using the criteria proposed by Mitsoulis [51] where $|\tau| \leq \tau_y$) in grey. It should be noted that the zones defined by $|\tau| \leq \tau_y$ are, technically, not "unyielded", which was highlighted by Mitsoulis and Zisis [52], as there will always be flow in these regions because of the bi-viscosity approximation used to model the Bingham fluid in the current study. These regions are, instead, essentially high-viscosity regions with slow-moving fluid which have been referred to as "Apparently Unyielded Regions (AUR)" [52]. It is evident from Figs. 3 and 4 that for $Bn = 0.5$ cases (for all nominal Rayleigh number $Ra$ and sidewall inclination angle $\varphi$ considered), the AURs are present across the whole of the trapezoidal cavity which is consistent with the observations of the local Nusselt number $Nu$ on the heated bottom wall where the flow essentially ceases above $Bn = 0.2$ and the heat transfer occurs by virtue of conduction. By definition, no AURs are present in the Newtonian (i.e., $Bn = 0$) cases. However, it is evident from Figs. 3 and 4 that for $Bn = 0.1$, $Ra = 10^5$ cases, the development of AURs can be observed in the acute angled corners (i.e., the corners formed by the adiabatic wall and the cooled inclined sidewalls) where there is a reduced propensity for flow, as indicated by the streamline pattern previously discussed. Furthermore, AURs have also been observed to originate at the centre of the adiabatic top wall and the centre of the heated bottom wall which is consistent with the symmetrical nature of the considered configuration and the resulting circulating regions.

### 3.5. Effects of Bingham number Bn

The effects of Bingham number $Bn$ on the nature of the heat and mass transfer in the trapezoidal cavity can further be shown through the variation of the mean Nusselt number $\overline{Nu}$ with Bingham number $Bn$, as shown for nominal Rayleigh number $Ra = 10^3$, $10^4$ and $10^5$ at nominal Prandtl number $Pr = 10^3$ for $\varphi = 30°$, $45°$ and $60°$ in Fig. 7a–c, respectively. Fig. 7a–c show that, for a given set of values of $Ra$, $Pr$ and $\varphi$, the mean Nusselt number $\overline{Nu}$ is found to decrease as Bingham number $Bn$ increases until the mean Nusselt number $\overline{Nu}$ plateaus to a constant value corresponding to the $\overline{Nu}$ value obtained for the pure conduction solution, once a threshold value of $Bn$ is obtained (i.e., for Bingham number $Bn \geq Bn_{max}$). For large values of Bingham number $Bn$, where the yield stress $\tau_y$ is sufficiently large such that the flow within the enclosure effectively vanishes and, thus, the heat transfer takes place only due to thermal conduction. As the thermal conduction transport is not altered by the variation of Rayleigh number $Ra$, the variation of $Ra$ does not alter $\overline{Nu}$ for $Bn \geq Bn_{max}$. Importantly, however, Fig. 7a–c show that an increase in Rayleigh number $Ra$ leads to an increase in the mean Nusselt number $\overline{Nu}$ for sufficiently low values of Bingham number $Bn$ where advection plays a key role in thermal transport. Moreover, the relative strength of the buoyancy force increases with increasing nominal Rayleigh number $Ra$ and, thus, the highest value of Bingham number for which advective transport plays a significant role in thermal transport also increases with an increase in $Ra$. This is reflected in the increase in $Bn_{max}$ with an increase in nominal Rayleigh number $Ra$. It can further be seen from Figs. 7a-c that for $Ra = 10^5$ cases, across all sidewall inclination angles $\varphi$, a hysteresis loop is observed (i.e., the branch of the variation of the mean Nusselt number $\overline{Nu}$ with increasing Bingham number $Bn$ is different from the branch of the variation of the mean Nusselt number $\overline{Nu}$ with decreasing Bingham number $Bn$). However, no evidence of hysteresis was observed for the Rayleigh number $Ra = 10^3$
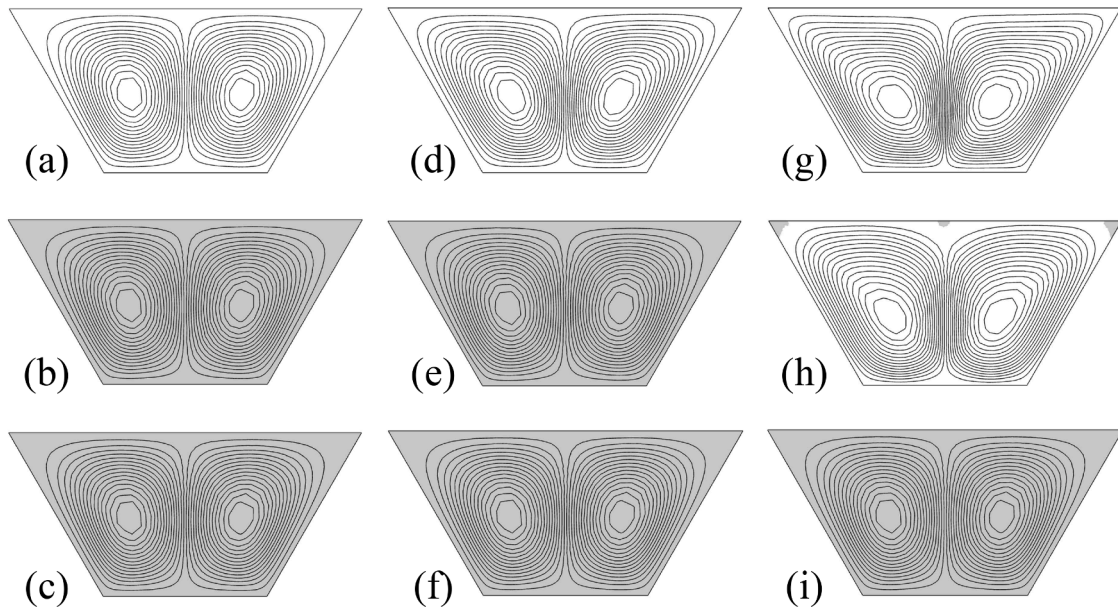
**Fig. 3.** Streamlines where $Pr = 10^3$ and $\varphi = 30°$ for (a) $Ra = 10^3$, $Bn = 0.0$, (b) $Ra = 10^3$, $Bn = 0.1$, (c) $Ra = 10^3$, $Bn = 0.5$, (d) $Ra = 10^4$, $Bn = 0.0$, (e) $Ra = 10^4$, $Bn = 0.1$, (f) $Ra = 10^4$, $Bn = 0.5$, (g) $Ra = 10^5$, $Bn = 0.0$, (h) $Ra = 10^5$, $Bn = 0.1$, and (i) $Ra = 10^5$, $Bn = 0.5$. The grey regions indicate the Apparently Unyielded Regions (AUR) [51].



**Fig. 4.** Streamlines where $Pr = 10^3$ and $\varphi = 60°$ for (a) $Ra = 10^3$, $Bn = 0.0$, (b) $Ra = 10^3$, $Bn = 0.1$, (c) $Ra = 10^3$, $Bn = 0.5$, (d) $Ra = 10^4$, $Bn = 0.0$, (e) $Ra = 10^4$, $Bn = 0.1$, (f) $Ra = 10^4$, $Bn = 0.5$, (g) $Ra = 10^5$, $Bn = 0.0$, (h) $Ra = 10^5$, $Bn = 0.1$, and (i) $Ra = 10^5$, $Bn = 0.5$. The grey regions indicate the Apparently Unyielded Regions (AUR) [51].

and $Ra = 10^4$ cases, across all sidewall inclination angles $\varphi$, considered. It should be noted that when moving along each branch of the variation of the mean Nusselt number $\overline{Nu}$ (i.e., for both increasing and decreasing Bingham number $Bn$), the results of the previous Bingham number $Bn$ case are used for the initial conditions. Importantly, this indicates that the initial conditions used have the potential to influence the resulting nature of the heat transfer behaviour in the range of Bingham number $Bn$ where the hysteresis loop occurs. It can further be observed from Fig. 7a–c that the range of Bingham number $Bn$ over which the observed hysteresis loop occurs decreases with increasing inclination angle $\varphi$ which indicates that the rheological behaviour of the fluid – and, therefore, the nature of the heat transfer in the fluid – is influenced not only by initial conditions employed but also by the geometrical configuration of the considered scenario.

The effect of Bingham number $Bn$ on the behaviour of the flow in the trapezoidal enclosure can be further illustrated by considering the non-dimensional vertical velocity $U_2 = u_2 L/\alpha$ at the vertical centreline (i.e., vertical line of symmetry) which is shown for Rayleigh number $Ra = 10^5$ and Prandtl number $Pr = 10^3$ for sidewall inclination angles $\varphi = 30°$, $45°$ and $60°$ in Fig. 8a–c, respectively. Fig. 8a–c show that the non-dimensional vertical velocity $U_2$ decreases with increasing nominal

Bingham number $Bn$. This corroborates the observations from Fig. 7a-c, which suggests that an increase in Bingham number $Bn$ indicates the strengthening of the flow resistance relative to buoyancy forces and this is reflected in a reduction in non-dimensional vertical velocity $U_2$ magnitude. Therefore, the advective transport weakens with increasing nominal Bingham number $Bn$. As such, this suggests that an increase in Bingham number $Bn$ eventually leads to a decrease in non-dimensional vertical velocity $U_2$ magnitude and, thus, conduction plays an increasingly important role for large values of $Bn$.

### 3.6. The effect of sidewall inclination angle $\varphi$

The effects of the sidewall inclination angle $\varphi$ on the behaviour of the heat transfer can be obtained by considering the variation of mean Nusselt number $\overline{Nu}$ with Bingham number $Bn$ for the sidewall inclination angles $\varphi = 30°$, $45°$ and $60°$, which is shown in Fig. 9. It is evident from Fig. 9 that an increase in the angle $\varphi$ leads to a decrease in the mean Nusselt number $\overline{Nu}$ which is due to the walls at temperature $T_C$ (i.e., the inclined to the vertical, cooled walls) becoming longer, resulting in a greater area for losing heat from the trapezoidal enclosure, and, therefore, a smaller heat flux is required for higher values of sidewall
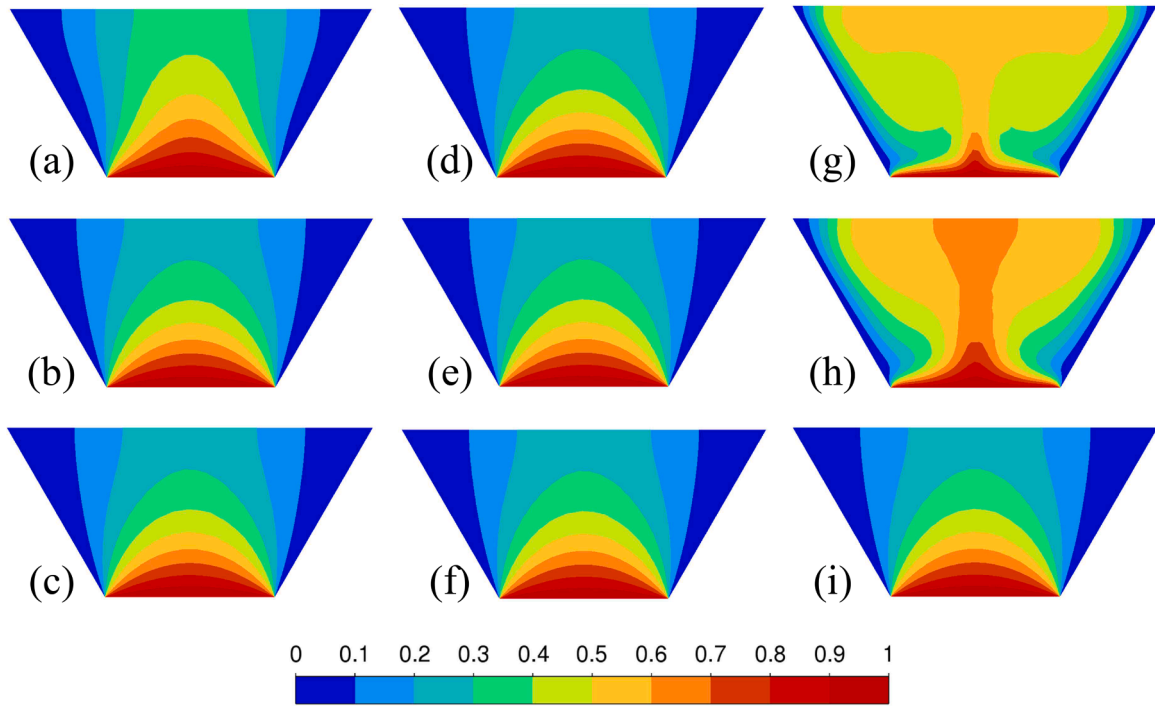
**Fig. 5.** Contours of non-dimensional temperature θ where $Pr = 10^3$ and $\varphi = 30°$ for (a) $Ra = 10^3$, $Bn = 0.0$, (b) $Ra = 10^3$, $Bn = 0.1$, (c) $Ra = 10^3$, $Bn = 0.5$, (d) $Ra = 10^4$, $Bn = 0.0$, (e) $Ra = 10^4$, $Bn = 0.1$, (f) $Ra = 10^4$, $Bn = 0.5$, (g) $Ra = 10^5$, $Bn = 0.0$, (h) $Ra = 10^5$, $Bn = 0.1$, and (i) $Ra = 10^5$, $Bn = 0.5$.
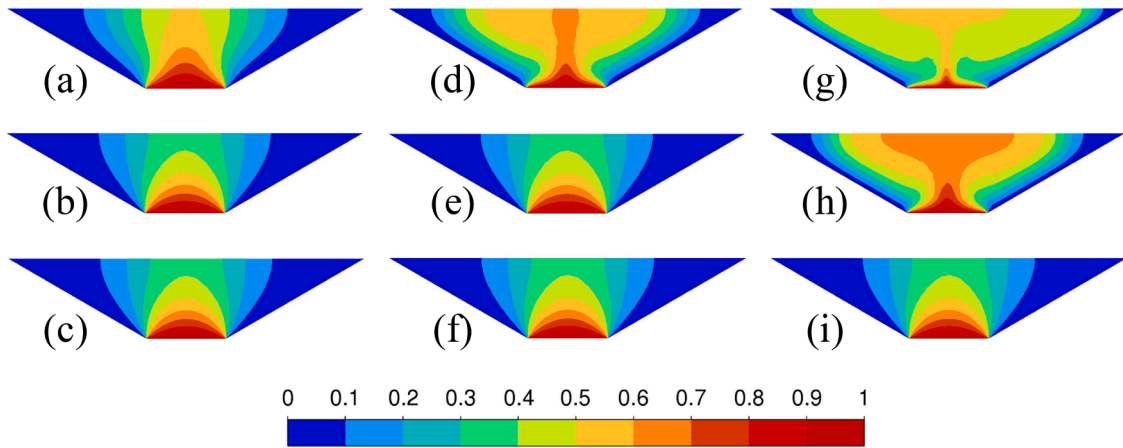


**Fig. 6.** Contours of non-dimensional temperature θ where $Pr = 10^3$ and $\varphi = 60°$ for (a) $Ra = 10^3$, $Bn = 0.0$, (b) $Ra = 10^3$, $Bn = 0.1$, (c) $Ra = 10^3$, $Bn = 0.5$, (d) $Ra = 10^4$, $Bn = 0.0$, (e) $Ra = 10^4$, $Bn = 0.1$, (f) $Ra = 10^4$, $Bn = 0.5$, (g) $Ra = 10^5$, $Bn = 0.0$, (h) $Ra = 10^5$, $Bn = 0.1$, and (i) $Ra = 10^5$, $Bn = 0.5$.

inclination angle φ to maintain the same temperature difference $\Delta T = (T_H - T_C)$ under steady state. However, it can further be seen from Fig. 9 that the range of Bingham number $Bn$ for which advective transport plays an important role in thermal transport increases with increasing inclination angle φ. This behaviour originates from the fact that AURs occupy a greater proportion of the domain for a smaller value of the inclination angle φ (see Figs. 3 and 4). Thus, the flow practically stops at a smaller value of Bingham number for smaller φ.

### 3.7. Correlation for the mean Nusselt number $\overline{Nu}$

The observed effects of Rayleigh number $Ra$, Bingham number $Bn$ and sidewall inclination angle φ on the heat transfer behaviour must be accounted for deriving the correlation for the mean Nusselt number $\overline{Nu}$. Previous analyses [8–12,14–19] have developed expressions for the mean Nusselt number $\overline{Nu}$ for Bingham fluids in different enclosures across a range of Rayleigh number $Ra$, Prandtl number $Pr$, and Bingham number $Bn$ based on scaling arguments [5,8]. The scaling arguments used in previous studies [5,8] are also applicable for the current analysis, and thus equipped by the scaling relations an expression can be proposed that varies in the region of Bingham number $0 \leq Bn \leq Bn_{max}$ accounting for the fall in mean Nusselt number $\overline{Nu}$ in this range and takes a constant value where Bingham number $Bn > Bn_{max}$. As such, the following expression, for the increasing $Bn$ branch, which follows previously proposed expressions [5,8] can be given as follows for trapezoidal enclosures:

$$\frac{\overline{Nu}}{\overline{Nu}_{COND}} = 1 + \left[\frac{\overline{Nu}_{Bn=0}}{\overline{Nu}_{COND}} - 1\right] \frac{2\left[1 - \left(Bn^*/Bn^*_{max}\right)^{c_1}\right]^{c_2}}{Bn^* + \sqrt{Bn^{*2} + 4}} \text{ for } \frac{\overline{Nu}}{\overline{Nu}_{COND}} > 1 \quad (4\text{i})$$

otherwise, $\dfrac{\overline{Nu}}{\overline{Nu}_{COND}} = 1$ (4ii)
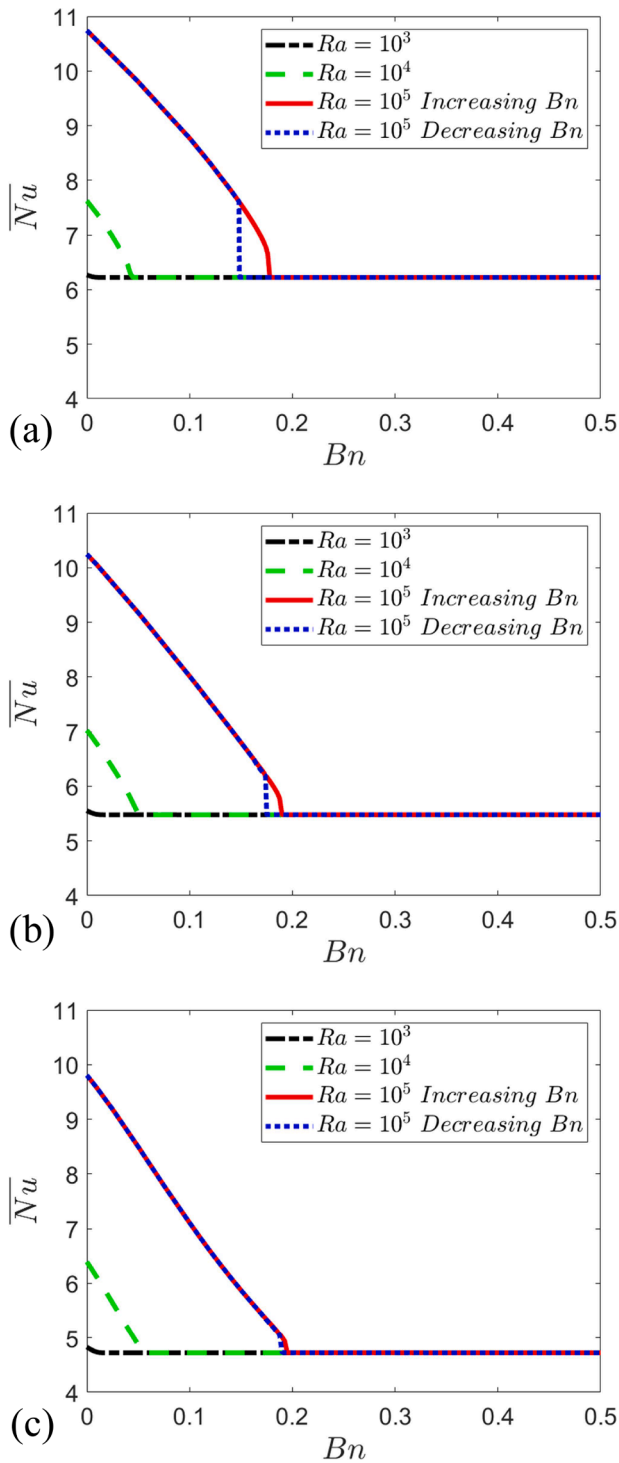
**Fig. 7.** Variations of the mean Nusselt number $\overline{Nu}$ on the hot bottom wall with Bingham number $Bn$ for $Ra = 10^3$, $10^4$ and $10^5$ where $Pr = 10^3$ for (a) $\varphi = 30°$, (b) $\varphi = 45°$, and (c) $\varphi = 60°$.

where $\overline{Nu}_{COND}$ is the value of $\overline{Nu}$ for corresponding pure conductive transport, $\overline{Nu}_{Bn=0}$ is the value of $\overline{Nu}$ for the $Bn = 0$ case (i.e., Newtonian case), $Bn^* = Bn/[(Ra/Pr)^{1/4}]$, $Bn^*_{max} = Bn_{max}/[(Ra/Pr)^{1/4}]$, and $c_1$ and $c_2$ are expression parameters. The mean Nusselt number for Newtonian fluids $\overline{Nu}_{Bn=0}$ can be expressed using the previous analyses by the present authors [43] as:

$$\overline{Nu}_{Bn=0} = C_1.(Ra/Pr)^{1/4} \text{ for } C_1.(Ra/Pr)^{1/4} > 1 \qquad (4\text{iii})$$
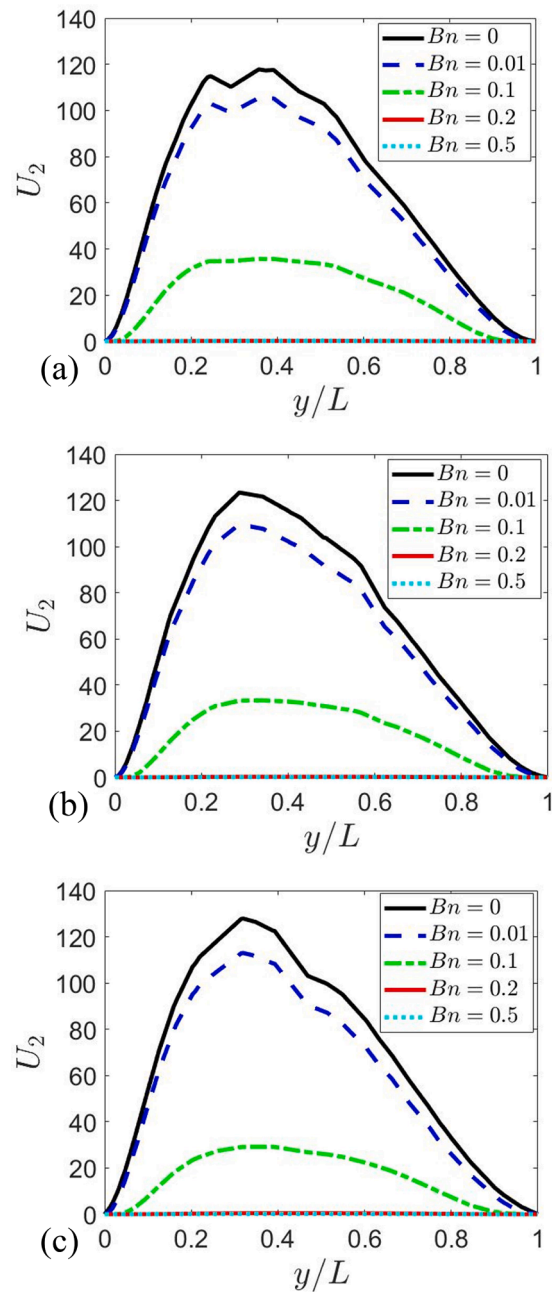


**Fig. 8.** Variation of non-dimensional vertical velocity $U_2 = u_2 L/\alpha$ along the vertical centreline for different Bingham numbers for $Ra = 10^5$ and $Pr = 10^3$ for (a) $\varphi = 30°$, (b) $\varphi = 45°$, and (c) $\varphi = 60°$.

$$\overline{Nu}_{Bn=0} = 1.0 \text{ for } C_1.(Ra/Pr)^{1/4} \le 1 \qquad (4\text{iv})$$

where $C_1 = 1.56(Ra^{-0.18})(Pr^{0.5})(1.5^{-\phi[rad]})$ is a correlation parameter. The expressions given by Eqs. 4i and 4ii are dependent upon the adequate representation of $Bn_{max}$. An expression for $Bn_{max}$, which extends upon a previous expression proposed for square enclosures [5,8] to application in trapezoidal enclosures, has been suggested in the following manner $Bn_{max} = (1 + C_{\varphi2})[0.0019 ln(Ra) - 0.0128]Ra^{0.55}Pr^{-0.50}$ where $C_{\varphi2} = 0.35\varphi[rad]^{0.5}$. It is evident from Fig. 10a–c that the expression given by Eq. 4i, when $c_1 = 0.6$ and $c_2 = 1.85Ra^{-0.1}$, generally provides a satisfactory qualitative and quantitative variation ($R^2 = 0.94$) of $\overline{Nu}/\overline{Nu}_{COND}$ for the range of Rayleigh number $Ra$, Bingham number $Bn$ and sidewall inclination angle $\varphi$ considered.
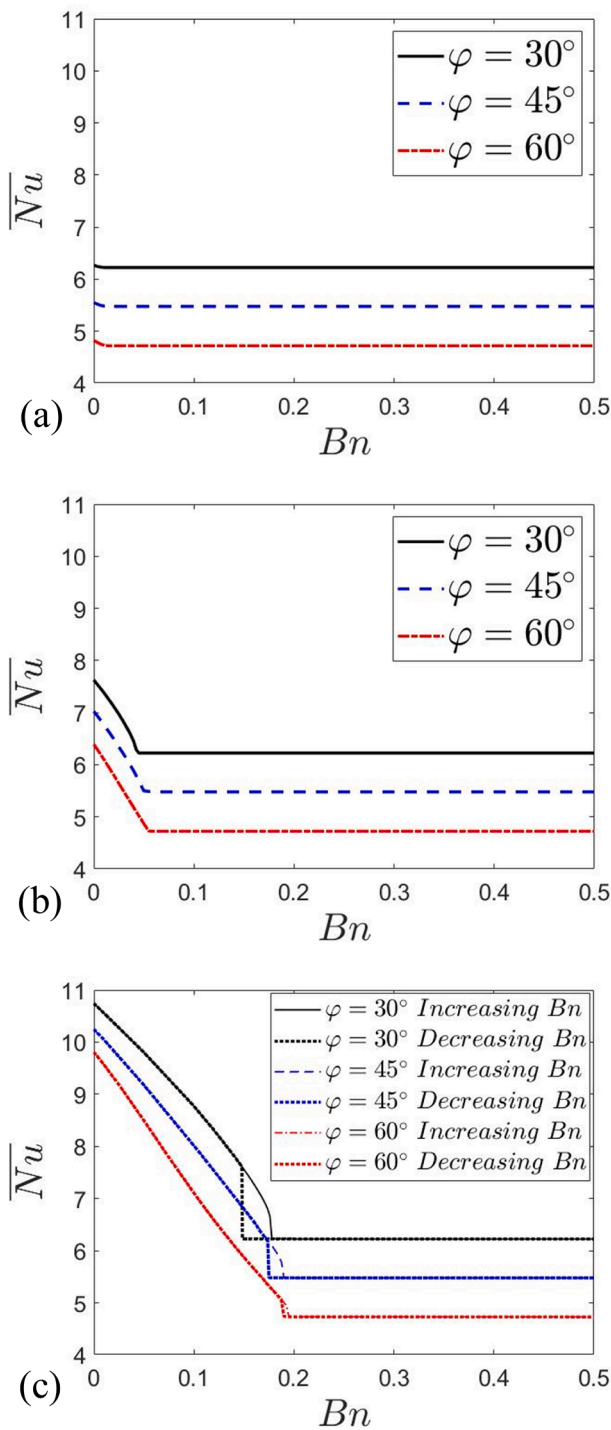
**Fig. 9.** The variation of mean Nusselt number $\overline{Nu}$ for the hot bottom wall with Bingham number $Bn$ for $\varphi = 30°$, $45°$ and $60°$ where $Pr = 10^3$ for (a) $Ra = 10^3$, (b) $Ra = 10^4$, and (c) $Ra = 10^5$.
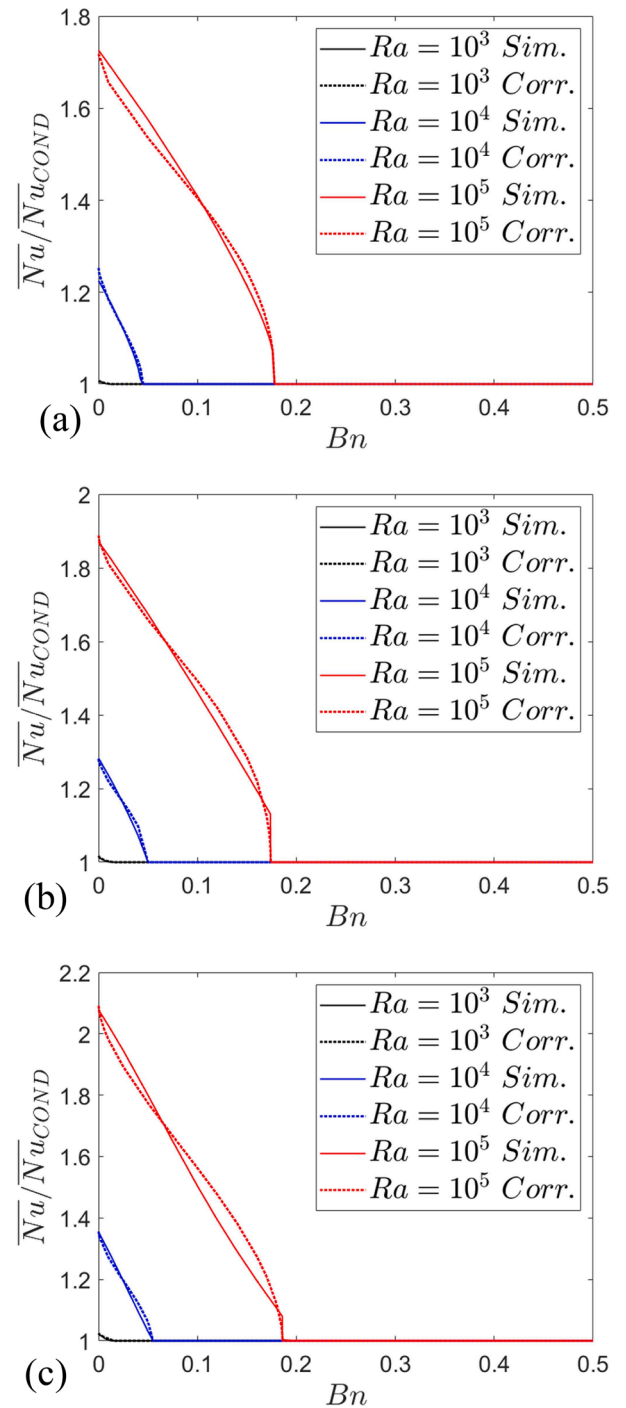


**Fig. 10.** The variation of $\overline{Nu}/\overline{Nu}_{COND}$ with Bingham number $Bn$ for $Ra = 10^3$, $10^4$ and $10^5$ where $Pr = 10^3$ for (a) $\varphi = 30°$, (b) $\varphi = 45°$, and (c) $\varphi = 60°$ for the increasing Bingham number $Bn$ branch along with the values from Eq. (4).

## 4. Conclusions

Laminar, steady-state, natural convection of Bingham fluids in trapezoidal enclosures with a heated bottom wall, cooled inclined sidewalls, and an adiabatic top has been analysed based on numerical simulations for a range of nominal Rayleigh number $Ra$ (i.e., $10^3 \leq Ra \leq 10^5$), Bingham number $Bn$ and sidewall inclination angle $\varphi$ (i.e., $30° \leq \varphi \leq 60°$) for a nominal Prandtl number of $Pr = 10^3$. The main conclusions are, as follows:

- The mean Nusselt number $\overline{Nu}$ increases with increasing Rayleigh number $Ra$ (up to a 71 % increase for $\varphi = 30°$ and up to 103 % increase for $\varphi = 60°$ between $Ra = 10^3$ and $10^5$) because of the strengthening of advective transport for small and moderate values of Bingham number.
- An increase in the sidewall inclination angle $\varphi$ leads to a decrease in the mean Nusselt number $\overline{Nu}$ (up to a 23% decrease for $Ra = 10^3$ and up to 4.7 % decrease for $Ra = 10^5$ between $\varphi = 30°$ and $\varphi = 60°$) due to an increase in the area for heat loss from the cavity.

- The value of the mean Nusselt number $\overline{Nu}$ was found to decrease with increasing Bingham number $Bn$ (up to a 2.3 % decrease for $Ra = 10^3$ and up to 52 % decrease for $Ra = 10^5$ between $Bn = 0$ and $Bn = Bn_{max}$). At high values of Bingham number $Bn$, the fluid flow practically ceases within the enclosure and heat transfer begins to take place due to thermal conduction and, therefore, the value of the mean Nusselt number $\overline{Nu}$ settles to a constant value corresponding to the pure conductive transport irrespective of the value of Rayleigh number $Ra$.
- It has also been found that for Rayleigh number $Ra = 10^5$ cases, across all inclination angles $\varphi$, a hysteresis loop is obtained. However, no evidence of hysteresis was observed for the Rayleigh number $Ra = 10^3$ and $Ra = 10^4$ cases, across all inclination angles $\varphi$, considered. Moreover, the range of Bingham number $Bn$ over which the observed hysteresis loop occurs decreases with increasing inclination angle $\varphi$.
- A correlation for $\overline{Nu}$, across the increasing Bingham number $Bn$ branch of the mean Nusselt number $\overline{Nu}$ variation, for the considered configuration accounting for the range of Rayleigh number $Ra$, and sidewall inclination angle $\varphi$ has been proposed based on scaling arguments. This correlation has been demonstrated to provide satisfactory predictions of both qualitative and quantitative variations of the mean Nusselt number $\overline{Nu}$.

## Ethics statement

This work did not involve any active collection of human data.

## Declaration of Competing Interest

The authors declare that they have no known competing financial interests or personal relationships that could have appeared to influence the work reported in this paper.

## Data availability

Data will be made available on request.

## References

[1] J. Zhang, D. Vola, I.A. Frigaard, Yield stress effects on Rayleigh–Bénard convection, J. Fluid Mech. 66 (2006) 389–419.
[2] N.J. Balmforth, A.C. Rust, Weakly nonlinear viscoplastic convection, J. Non-Newtonian Fluid Mech. 158 (2009) 36–45.
[3] A. Vikhansky, Thermal convection of a viscoplastic liquid with high Rayleigh and Bingham numbers, Phys. Fluids 21 (2009), 103103.
[4] Vikhansky, On the onset of natural convection of Bingham liquid in rectangular enclosures, J. Non-Newtonian Fluid Mech. 165 (2010) 1713–1716.
[5] O. Turan, N. Chakraborty, R.J. Poole, Laminar natural convection of Bingham fluids in a square enclosure with differentially heated side walls, J. Non-Newtonian Fluid Mech. 165 (2010) 901–913.
[6] M. Darbouli, C. Métivier, J.-M. Piau, A. Magnin, A. Abdelali, Rayleigh-Bénard convection for viscoplastic fluids, Phys. Fluids 25 (2013), 023101.
[7] Z. Kebiche, C. Castelain, T. Burghelea, Experimental investigation of the Rayleigh–Bénard convection in a yield stress fluid, J. Non-Newtonian Fluid Mech. 203 (2014) 9–23.
[8] O. Turan, N. Chakraborty, R.J. Poole, Laminar Rayleigh-Bénard convection of yield stress fluids in a square enclosure, J. Non-Newtonian Fluid Mech. 171 (2012) 83–96.
[9] O. Turan, A. Sachdeva, R.J. Poole, N. Chakraborty, Laminar natural convection of Bingham fluids in a square enclosure with vertical walls subjected to constant heat flux, Numer. Heat Transf. Part A Appl. 60 (2011) 381–409.
[10] S. Yigit, R.J. Poole, N. Chakraborty, Laminar natural convection of Bingham fluids in inclined differentially heated square enclosures subjected to uniform wall temperatures, J. Heat Trans. 137 (2015), 52504-052504-052512.
[11] S. Yigit, R.J. Poole, N. Chakraborty, Effects of aspect ratio on natural convection of Bingham fluids in rectangular enclosures with differentially heated horizontal walls heated from below, Int. J. Heat and Mass Trans. 80 (2015) 727–736.
[12] S. Yigit, N. Chakraborty, Influences of aspect ratio and wall boundary condition on laminar Rayleigh–Bénard convection of Bingham fluids in rectangular enclosures, Int. J. Numer. Heat Fluid Flow 27 (2017) 310–333.
[13] M.A. Hassan, M. Pathak, M.K. Khan, Rayleigh–Benard convection in Herschel–Bulkley fluid", J. Non-Newtonian Fluid Mech. 226 (2015) 32–45.
[14] S. Yigit, S. Chen, P. Quinn, N. Chakraborty, Numerical investigation of laminar Rayleigh-Bénard convection of Bingham fluids in square cross-sectioned cylindrical enclosures, Int. J. Therm. Sci. 110 (2016) 356–368.
[15] S. Yigit, N. Chakraborty, Laminar natural convection of Bingham fluid in cylindrical square cross-sectioned cylindrical annular enclosures with differentially heated vertical walls subjected to constant heat fluxes, Heat Trans. Eng. 38 (2017) 1171–1188.
[16] S. Yigit, T. Foxon, N. Chakraborty, Influences of boundary condition on laminar natural convection of bingham fluids in square cross-sectioned cylindrical annular enclosures with differentially heated vertical walls, Heat Trans. Eng. (2017) 1–20.
[17] S. Yigit, N. Chakraborty, Numerical investigation of aspect ratio influences on Rayleigh-Bénard convection of Bingham fluids in vertical cylindrical annuli, Int. J. Num. Methods Heat Fluid Flow 29 (2019) 251–279.
[18] S. Yigit, N. Chakraborty, Natural convection of Bingham fluids in rectangular cross-sectional cylindrical annuli with differentially heated vertical walls, Int. J. Num. Methods Heat Fluid Flow 29 (2019) 43–77.
[19] S. Yigit, J. Hasslberger, N. Chakraborty, M. Klein, Effects of Rayleigh-Bénard convection on spectra of viscoplastic fluids, Int. J. Heat Mass Trans. 147 (2020), 118947.
[20] M.S. Aghighi, A. Ammar, H. Masoumi, A. Lanjabi, Rayleigh–Bénard convection of a viscoplastic liquid in a trapezoidal enclosure, Int. J. Mech. Sci. 180 (2020), 105630.
[21] E.C. Bingham, An investigation of the laws of plastic flow, Bull. Bureau Stand. 13 (2) (1916) 309–353.
[22] A.K. Hussein, L. Kolsi, R. Chand, S. Sivasankaran, R. Nikbakhti, D. Li, M. Borjini, H. Ben Aïssia, Three-dimensional unsteady natural convection and entropy generation in an inclined cubical trapezoidal cavity with an isothermal bottom wall, Alex. Eng. J. 55 (2016) 741–755.
[23] L. Iyican, L.C. Witte, Y. Bayazitoglu, An experimental study of natural convection in trapezoidal enclosures, J. Heat Trans. 102 (1980) 648–653.
[24] S.W. Lam, R. Gani, J.G. Simons, Experimental and numerical studies of natural convection in trapezoidal cavities, J. Heat Trans. 111 (1989) 372–377.
[25] Y.E. Karyakin, Transient natural convection in prismatic enclosures of arbitrary cross-section, Int. J. Heat Mass Trans 32 (1989) 1095–1103.
[26] T.S. Lee, Numerical experiments with fluid convection in tilted nonrectangular enclosures, Numer. Heat Trans. A 19 (1991) 487–499.
[27] T.S. Lee, Computational and experimental studies of convective fluid motion and heat transfer in inclined non-rectangular enclosures, Int. J. Heat Fluid Flow 5 (1984) 29–36.
[28] M. Peric, Natural convection in trapezoidal cavities, Numer. Heat Trans. A 24 (1993) 213–219.
[29] H. Sadat, P. Salagnac, Further results for Laminar natural convection in a two-dimensional trapezoidal enclosure, Numer. Heat Trans. A 27 (1995) 451–459.
[30] R.A. Kuyper, C.J. Hoogendoorn, Laminar natural convection flow in trapezoidal enclosures, Numer. Heat Trans. A 28 (1995) 55–67.
[31] F. Moukalled, S. Acharya, Buoyancy-induced heat transfer in partially divided trapezoidal cavities, Numer. Heat Trans. A 32 (1997) 787–810.
[32] F. Moukalled, S. Acharya, Natural convection in trapezoidal cavities with baffles mounted on the upper inclined surfaces, Numer. Heat Trans. A 37 (2000) 545–565.
[33] F. Moukalled, S. Acharya, Natural convection in a trapezoidal enclosure with offset baffles, AIAA J. Thermophys. Heat Trans. 15 (2001) 212–218.
[34] F. Moukalled, M. Darwish, Natural convection in partitioned trapezoidal cavity heated from the side, Num. Heat Trans Part A 43 (2010) 543–563.
[35] A. da Silva, É. Fontana, F. Marcondes, Numerical investigation of several physical and geometric parameters in the natural convection into trapezoidal cavities, Int. J. Heat Mass Transf. 55 (2012) 6808–6818.
[36] T. Basak, S. Roy, I. Pop, Heat flow analysis for natural convection within trapezoidal enclosures based on heatline concept, Int. J. Heat Mass Trans. 52 (2009) 2471–2483.
[37] N.I. Tracy, D.W. Crunkleton, Oscillatory natural convection in trapezoidal enclosures, Int. J. Heat Mass Transf. 55 (2012) 4498–4510.
[38] S.A.M. Mehryan, M. Ghalambaz, R.K. Feeoj, A. Hajjar, M. Izadif, Free convection in a trapezoidal enclosure divided by a flexible partition, Int. J. Heat Mass Transf. 149 (2020), 119186.
[39] R.U. Haq, S.N. Kazmi, T. Mekkaoui, Thermal management of water based SWCNTs enclosed in a partially heated trapezoidal cavity via FEM, Int. J. Heat Mass Transf. 112 (2017) 972–982.
[40] R.U. Haq, S. Aman, Water functionalized CuO nanoparticles filled in a partially heated trapezoidal cavity with inner heated obstacle: FEM approach, Int. J. Heat Mass Transf. 128 (2019) 401–417.
[41] H. Saleh, R. Roslan, I. Hashim, Natural convection heat transfer in a nanofluid-filled trapezoidal enclosure, Int. J. Heat Mass Transf. 54 (2011) 194–201.
[42] M.H. Esfe, A.A.A. Arani, W. Yan, H. Ehteram, A. Aghaie, M. Afrand, Natural convection in a trapezoidal enclosure filled with carbon nanotube–EG–water nanofluid, Int. J. Heat Mass Trans. 92 (2016) 76–82.
[43] S.P. Malkeson, S. Alshaaili, N. Chakraborty, Numerical investigation of steady state laminar natural convection of power-law fluids in side-cooled trapezoidal enclosures heated from the bottom, Numer. Heat Trans. Part A (2023).
[44] E.J. O'Donovan, R.I. Tanner, Numerical study of the Bingham squeeze film problem, J. Non-Newtonian Fluid Mech. 15 (1984) 75–83.
[45] T.C. Papanastasiou, Flows of materials with yield, J. Rheol. 31 (1984) 385–404.
[46] J. Peixinho, C. Desaubry, M. Lebouche, Heat transfer of a non-newtonian fluid (Carbopol aqueous solution) in transitional pipe flow, Int. J. Heat Mass Trans. 51 (2008) 198–209.

[47] ANSYS fluent user's guide, 2020 R2.

[48] S.V. Patankar, Numerical Heat Transfer and Fluid Flow, Hemisphere, Washington D.C., 1980.

[49] G. de Vahl Davis, Natural convection of air in a square cavity: a benchmark solution, Int. J. Numer. Methods Fluids 3 (1993) 249–264.

[50] D. Vola, L. Boscardin, J.C. Latché, Laminar unsteady flows of Bingham fluids: a numerical strategy and some benchmark results, J. Computat. Phys. 187 (2003) 441–456.

[51] E. Mitsoulis, Flows of viscoplastic materials: models and computations, in: D. M. Binding, N.E. Hudson, R. Keunings (Eds.), Rheology Reviews, 2007, pp. 135–178.

[52] E. Mitsoulis, T. Zisis, Flow of Bingham plastics in a lid-driven square cavity, J. Non-Newtonian Fluid Mech. 101 (2001) 173–180.